Cytoskeletal Regulation Couples LFA-1 Conformational Changes to Receptor Lateral Mobility and Clustering

Christopher W. Cairo, Rossen Mirchev, and David E. Golan

Supplemental Experimental Procedures

Section S1. SPT Data Analysis

Particle trajectories were analyzed using an MSD analysis, as described by Saxton and Jacobson.[1] High-speed video frames (1000 FPS) were analyzed using a pattern-matching algorithm implemented in Metamorph (Universal Imaging). The trajectory was then read into a custom MATlab program and converted to a mean square displacement (MSD) vs. time interval curve. MSD was calculated as the average displacement of a given time interval averaged over all increments. The MSD vs. time interval curve was then analyzed to determine microdiffusion (D_{micro}) and macrodiffusion (D_{macro}) coefficients.

Section S2. Microdiffusion Fit

Micro-diffusion coefficients were calculated by performing a linear fit of the first four increments of the MSD vs. time interval curve (4 ms). Therefore, the slope of the fit represented the average diffusion coefficient over this short time interval. Fit values are given in the accompanying spreadsheet.

Section S3. Macrodiffusion Fit

Macro-diffusion coefficients were calculated by fitting the initial third of the MSD vs. time interval curve to the following equation:

$$< r^2 >= 4Dt^{\alpha} \quad (1)$$

Here, $<r^2>$ is the MSD, t is the time interval, D is the time-dependent diffusion coefficient (D_{macro}), and the α coefficient classifies the mode of anomalous diffusion.[2] Fit values with $\alpha < 0.7$ are considered to represent confined or corralled motion, values with $0.7 < \alpha < 1.2$ are consistent with brownian diffusion, and values with $\alpha > 1.2$ are considered to represent flow diffusion.[1] Fit values are given in the accompanying spreadsheet.

Section S4. Flow Diffusion Fit

An additional model for fitting treats diffusion with a positive flow component as:

$$< r^2 >= 4Dt + vt^2 \quad (2)$$

Again, $<r^2>$ is the MSD, t is the time interval, D is the diffusion coefficient (D_{flow}), and v is the speed of directed motion. Both the time-dependent diffusion and flow diffusion models separate any flow component of the trajectory from the diffusion term into α or v, respectively, and should counter artifacts due to cell motility (Figure S3). This model has been previously used to analyze LFA-1 trajectories.[3]

Section S5. Deconvolution of Subpopulations

Results of the macro-diffusion analysis were computed and plotted as a histogram and entered as the input to a custom MATlab program. Each point of the population was then used to construct a density estimation using standard methods.[4] Briefly, each point was treated as representing a portion of a population in either a normal (eq. 3) or logarithmic normal distribution (eq. 4). The population density of these distributions could be represented by:

$$d_N = Ae^{-\frac{(x-x_0)^2}{2c^2}} \qquad \text{or} \tag{3}$$

$$d_L = Ae^{-\frac{(\ln x-\ln x_0)^2}{2c^2}} \tag{4}$$

where x_0 is the center of the distribution, A is a normalization constant, and c is the variance of the distribution. For a normal distribution, the variance, σ_N, is given by:

$$\sigma_N(x) = c \tag{5}$$

For the logarithmic normal distribution:

$$\sigma_L(x) = x_0\sigma_N(x) = x_0c \tag{6}$$

We found that our D_{macro} data were logarithmically distributed, and we therefore analyzed the population density using d_L (eq. 4). The total population density was estimated as the sum of many component distributions of the same construction centered at their respective values provided by the D_{macro} fit results. The critical parameter in the density estimation is c, sometimes referred to as the 'bandwidth' for density estimation. In general, we used the Simple Normal Reference (c_{SNR}) to estimate c.[4] Finally, the standard error could be calculated from the variance, σ, as:

$$SEM = \frac{\sqrt{\sigma}}{\sqrt{N_p}} \tag{7}$$

for a given number of points in the population, N_p.

To deconvolute constituent subpopulations, we treated the total estimated density as the superposition of 1-3 individual populations:

$$d_{total} = d_i + d_c + d_m \tag{8}$$

where d_i is the density of the immobile peak, d_c is the density of the confined peak, and d_m is the density of the mobile peak. For each subpopulation density (d_i, d_c, d_m), the normalization parameter A and the center of the peak, x_0, were fit as independent variables. To perform the fits with the minimum number of variables, we fit a single value of c for any total density estimation such that:

$$c_i = c_c = c_m \tag{9}$$

The normalization parameter A for each subpopulation was used to determine the relative proportions of each peak in the total population. The only boundaries employed for the subpopulation fits were used for three-peak fits. In these calculations a restriction was added only for the *immobile* peak. Due to this peak's small relative area and inconsistent appearance among conditions, it was restricted to $0.02 < x_0 < 0.17$ [x 10^{-10} cm^2sec^{-1}].

Although several data sets could be marginally better fit with a three-peak analysis, the major findings from our experiments remained unchanged using a two-peak analysis. Therefore, in the absence of greater resolution in the diffusion profiles, we

chose to use a two-peak analysis for all data sets. For a comparison of two versus three-peak analysis, see Figure S2.

To compute weighted averages of the D_{micro} and α parameters for each D_{macro} subpopulation, the fit values of a given subpopulation were used to select data points most representative of the peak. To do this, the peak function was normalized to 1, and any values greater than $d = 0.65$ were used to compute a mean value. These values were computed as the arithmetic mean, and error is reported as the standard error of the mean. The number of values used to compute the weighted mean in each subpopulation is reported as N_w. Results of population fitting and weighted values for all individual subpopulations are given in the accompanying table (Table S2). The mobile and immobile peak centers were clearly and consistently resolved within each cell type (see Figure S4).

Section S6. Density of Bead Labels

We estimated an upper limit for the number of ICAM-1 sites on the polystyrene beads used for SPT experiments. We consider this an upper limit since an undetermined portion of ICAM-1 sites will be inaccessible to surface binding due to non-specific adsorption and the porous nature of the polystyrene beads. The number of ICAM-1 molecules used for a single preparation was approximately 8×10^{11} (0.1×10^{-6} g / 76 kDa * N_A). The number of beads used was 4.6×10^8 (10^{-3} mL * 4.55×10^{10} beads/mL). Therefore, the upper limit of ICAM-1 binding sites per bead was 1700 (8×10^{11} ICAM / 4.6×10^8 beads). The surface area of a single bead is approximated by:

$$SA_{bead} = 4\pi\left(\frac{d}{2}\right)^2 = \pi\left(d^2\right) \tag{10}$$

where d is the bead diameter (0.992 μm). Here, $SA_{bead} = 3.1\ \mu m^2$. Only a portion of the total bead surface can contact the cell; therefore, the upper limit of the contact area would be half of the bead surface area, or:[5]

$$CA_{bead} = \frac{1}{2}\pi\left(d^2\right) \tag{11}$$

The density of the ICAM-1 sites can be calculated by dividing the number of ICAM-1 sites on a single bead by the surface area of the bead (sites/SA_{bead}). In our experiments, the ICAM-1 site density was less than 560 sites/μm^2; the bead contact area was less than 1.5 μm^2; therefore, the upper limit of ICAM-1 sites per bead contact area was 870 ICAM-1 sites/contact. The actual site density is likely to be much lower, due to non-specific adsorption, the non-uniform bead surface, and a contact area that was less than ½ of the bead surface area.

Lymphocyte LFA-1-ICAM-1 adhesion requires a site density of ~10^4 sites/μm^2; therefore, the density on individual beads is at least 12-fold less than the physiologically required density of sites.[6] The density used was experimentally determined to be the minimum necessary to achieve specific labeling of cells.

A high ICAM-loading control had a 10-fold greater density of ICAM sites (less than 5600 sites/μm^2). These beads showed a large immobile subpopulation (50%) with a 4-fold lower diffusion coefficient compared to the low density beads used for other experiments.

Supplemental References

1. Saxton, M.J. & Jacobson, K. Single-particle tracking: Applications to membrane dynamics. *Annu. Rev. Biophys. Biomol. Struct.* **26**, 373-399 (1997).

2. Mirchev, R. & Golan, D.E. Single-particle tracking and laser optical tweezers studies of the dynamics of individual protein molecules in membranes of intact human and mouse red cells. *Blood Cells Molecules and Diseases* **27**, 143-147 (2001).

3. Kucik, D.F., Dustin, M.L., Miller, J.M., & Brown, E.J. Adhesion-activating phorbol ester increases the mobility of leukocyte integrin LFA-1 in cultured lymphocytes. *J. Clin. Invest.* **97**, 2139-2144 (1996).

4. Sheather, S.J. Density estimation. *Statistical Science* **19**, 588-597 (2004).

5. Thoumine, O. & Meister, J.J. A probabilistic model for ligand-cytoskeleton transmembrane adhesion: Predicting the behavior of microspheres on the surface of migrating cells. *J. Theor. Biol.* **204**, 381-392 (2000).

6. Dustin, M.L. & Springer, T.A. Lymphocyte function associated antigen-1 (LFA-1) interaction with intercellular-adhesion molecule-1 (ICAM-1) is one of at least 3 mechanisms for lymphocyte adhesion to cultured endothelial-cells. *J. Cell Biol.* **107**, 321-331 (1988).

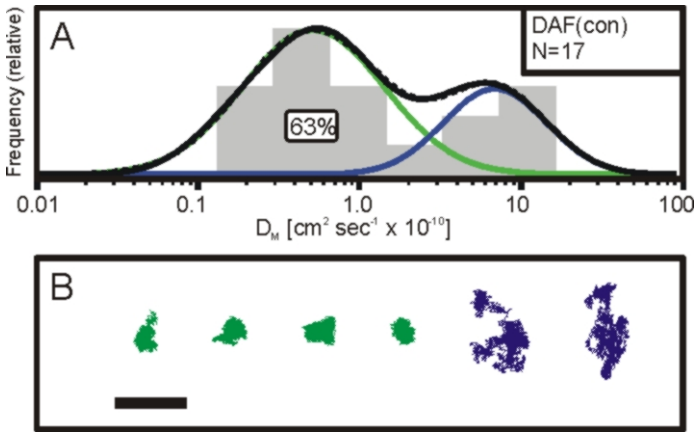

Figure S1. Diffusion of a GPI-Linked Protein on Jurkat Cells

Cells were labeled with beads coated with α-DAF F(ab)' (clone BRIC216, 0.1 μg) using the same protocol as for LFA-1 labeling. Cells were untreated controls (HBSSB with 0.1% DMSO). Note that these trajectories have the largest D_{micro} (17 ± 0.8 x 10^{-10} cm^2sec^{-1}) and D_{macro} (2.9 ± 0.9 x 10^{-10} cm^2sec^{-1}) coefficients measured. Additionally, the weighted values from subpopulation analysis demonstrate that DAF motion in the membrane is very different from LFA-1: The slow-diffusing peak at 0.5 x 10^{-10} cm^2sec^{-1} has a significantly reduced α value (0.4 ± 0.1) but maintains a microdiffusion value similar to the mobile peak (16 ± 1 x 10^{-10} cm^2sec^{-1}). This is in contrast to all LFA-1 labels, where the microdiffusion coefficients tend to be significantly reduced for the slowly diffusing populations, or else both populations have very low microdiffusion coefficients. Scale bar is 1 μm.

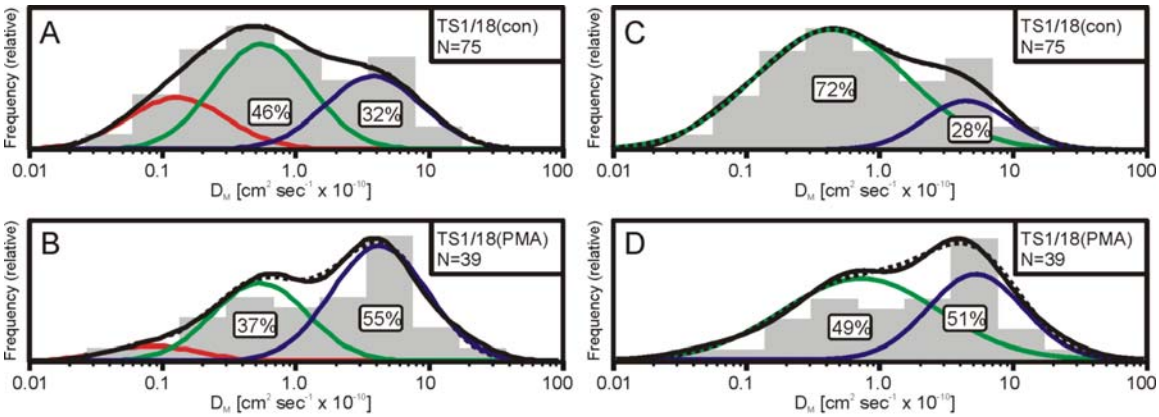

Figure S2. Comparison of 3-Peak and 2-Peak Analysis of TS1/18 Data

Although most of our data sets were fitted well using 2-peak analysis, analysis of some data sets suggested the possibility of more than two subpopulations in the diffusion profile. Treatment of these data for three-peak deconvolution provided a smaller variance of each subpopulation, and therefore less overlap between peaks. However, even if the third subpopulation was actually present, it was not well resolved. In general, the mobile population was well resolved in all of our data sets, and we focused our analysis on characterizing this subpopulation. The major conclusions of our analysis were not changed by the presence or absence of a third subpopulation.

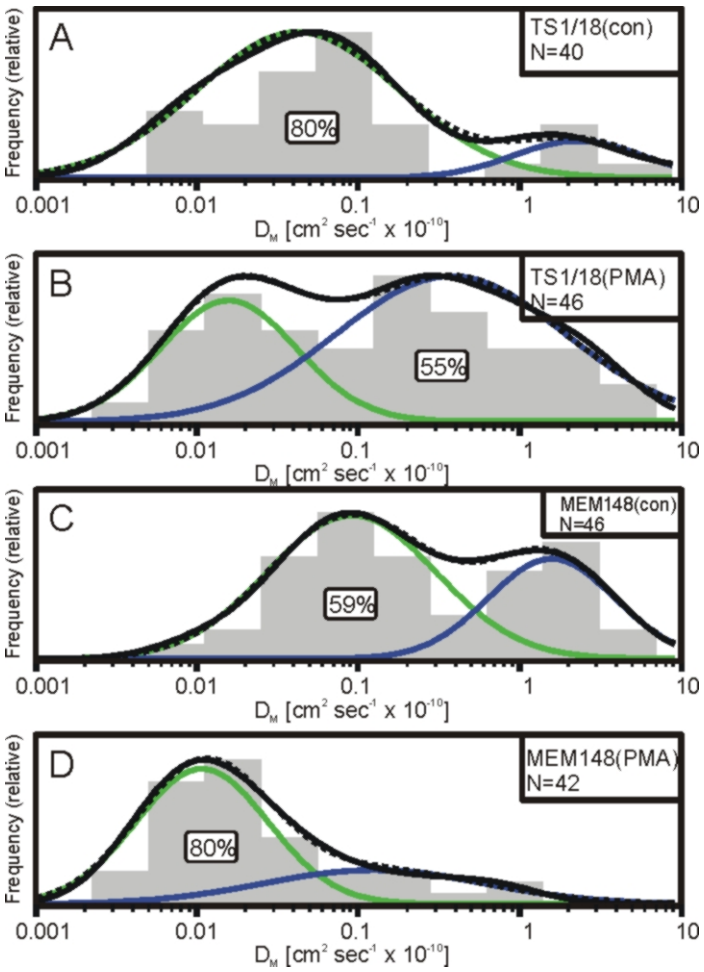

Figure S3. Flow Diffusion Analysis of PBL Results

Inspection of trajectories from PBL suggested an increased number of particles undergoing directed diffusion (Figure 6E). Observations of PBL under conditions used for experiments confirmed that some cells are highly motile (as much as ~ 100 nm sec^{-1}, data not shown). Jurkat cells were not observed to migrate under any conditions used. Analysis of trajectories using the time-dependent diffusion coefficient (eq. 1, above) should indicate directed motion by an α term larger than 1. Indeed, we observed that 35 – 57 % of trajectories on these cells had $\alpha > 1.2$. An alternative analysis for data of this type is a flow-diffusion model (eq. 2, above).[3] Using this model to analyze the PBL results yielded the same general conclusions: TS1/18 labels showed an increased mobile population after PMA treatment, while MEM148 labels were more mobile on resting cells but entirely immobile on activated cells. Although both models fit the data, the flow model provided a determination of the magnitude of flow observed. The largest of these values corresponded to ~ 50 nm sec^{-1}. Therefore, while cell motility appeared to contribute to the observed trajectories, both of the models accounted for this contribution and were able to separate D_{macro} from the directed component as either the α or v terms, respectively (see above). Note that the axis in Figure S3 is shifted by one log unit from that in Figure 6.

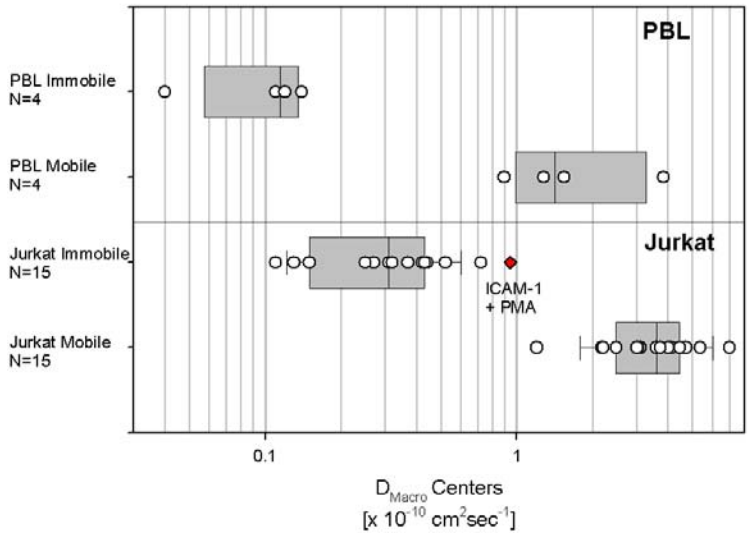

Figure S4. Resolution of Subpopulations

Our analysis of the SPT data for LFA-1 deconvolved the trajectories into 'mobile' and 'immobile' populations by fitting two independent log-normal distributions within the distribution of lateral diffusion coefficients (see Section S5). While there were some regions of overlap between the tails of these populations, the centers of the populations *did not overlap* between conditions and showed a large (ca. 12-fold) separation within any given condition. The values of all these fits are found in Table S2. By examining all of the conditions within each cell type, we measured the average and standard error of the fit centers of the mobile and immobile populations. This treatment showed that, in Jurkat cells, the immobile populations were centered at 0.30 +/- 0.05 x 10^{-10} cm^2sec^{-1} (range, 0.1–0.72) while the mobile populations were centered at 3.6 +/- 0.4 x 10^{-10} cm^2sec^{-1} (range, 1.2–7.0) for 15 different conditions (also, see below). For PBL, the values were 0.10 +/- 0.02 x 10^{-10} cm^2sec^{-1} (range, 0.04–0.14) for the immobile populations and 1.9 +/- 0.7 x 10^{-10} cm^2sec^{-1} (range, 0.9–3.8) for the mobile populations among 4 conditions. Based on this calculation, we argue that mobile and immobile populations were clearly resolved both *absolutely* and *relatively*. For Jurkat cells, the closest overlap between the two ranges was 1.7–fold, and the means were separated by 12–fold; in PBL, the closest overlap was 6–fold and the means were separated by 19–fold. In addition, we feel it is more appropriate to treat the *relative* differences within a single condition or label, and for Jurkat and PBL, the relative difference ranged between 7– and 28–fold.

We note that there was an important exception to the population separation rule stated above. In the singular case of ICAM-1 labeled beads on activated Jurkat cells, we observed a major population centered at 0.9 x 10^{-10} cm^2sec^{-1}, and this was the fastest population on these cells. This case is unique, as it was centered between the mobile and immobile ranges for Jurkat. However, we note that the trajectories comprising this population had an unusually low D_{micro} value, 3.1 +/- 0.6 x 10^{-10} cm^2sec^{-1}, whereas other mobile peaks had D_{micro} values of 10.6 +/- 0.6 x 10^{-10} cm^2sec^{-1} and immobile peaks had D_{micro} values of 4.6 +/- 0.5 x 10^{-10} cm^2sec^{-1}. We therefore considered the peak centered at D_{macro} = 0.9 x 10^{-10} cm^2sec^{-1} to be immobile, as discussed in the text.